Published in final edited form as:
Aging Cell. 2013 June ; 12(3): 478–488. doi:10.1111/acel.12072.

Balance between autophagic pathways preserves retinal homeostasis

Natalia-Rodríguez-Muela[1], **Hiroshi Koga**[2], **Lucía García-Ledo**[1], **Pedro de la Villa**[3], **Enrique J. de la Rosa**[4], **Ana María Cuervo**[2,#], and **Patricia Boya**[1,#]

[1]Department of Cellular and Molecular Biology, CIB, CSIC, Ramiro de Maeztu 9, E-28040 Madrid, Spain.

[2]Department of Developmental and Molecular Biology and Institute for Aging Studies, Albert Einstein College of Medicine, Bronx, New York 10461, USA.

[3]Department of Physiology, Universidad de Alcalá, E-28871 Alcalá de Henares, Spain.

[4]3D Lab, Department of Cellular and Molecular Medicine, CIB, CSIC, Ramiro de Maeztu 9, E-28040 Madrid, Spain.

Summary

Aging contributes to the appearance of several retinopathies and is the largest risk factor for aged-related macular degeneration, major cause of blindness in the elderly population. Accumulation of undegraded material as lipofuscin represents a hallmark in many pathologies of the aged eye. Autophagy is a highly conserved intracellular degradative pathway that plays a critical role in the removal of damaged cell components to maintain the cellular homeostasis. A decrease in autophagic activity with age observed in many tissues has been proposed to contribute to the aggravation of age-related diseases. However, the participation of different autophagic pathways to the retina physiopathology remains unknown. Here we describe a marked reduction in macroautophagic activity in the retina with age, which coincides with an increase in chaperone-mediated autophagy (CMA). This increase in CMA is also observed during retinal neurodegeneration in the *Atg5*$^{flox/flox}$; nestin-*Cre* mice, a mouse model with downregulation of macroautophagy in neuronal precursors. In contrast to other cell types, this autophagic cross-talk in retinal cells is not bi-directional and CMA inhibition renders cone photoreceptor very sensitive to stress. Temporal and cell-type specific differences in the balance between autophagic pathways may be responsible for the specific pattern of visual loss that occurs with aging. Our results show for the first time a cross-talk of different lysosomal proteolytic systems in the retina during normal aging and may help the development of new therapeutic intervention for age-dependent retinal diseases.

Keywords

Retina; aging; autophagy; chaperone-mediated autophagy; photoreceptor; lipofuscin

[#]**Corresponding authors:** Dr. Patricia Boya. Department of Cellular and Molecular Biology, CIB, CSIC, Ramiro de Maeztu 9, E-28040 Madrid, Spain. patricia.boya@csic.es. Dr. Ana María Cuervo. Department of Developmental and Molecular Biology and Institute for Aging Studies, Albert Einstein College of Medicine, Bronx, New York 10461, USA. ana-maria.cuervo@einstein.yu.edu.. nrodriguez@cib.csic.es hiroshi.koga@einstein.yu.edu lgarcile@cib.csic.es, pedro.villa@uah.es, ejdelarosa@cib.csic.es, ana-maria.cuervo@einstein.yu.edu patricia.boya@csic.es

Author's contributions NRM performed most of the research and wrote the first draft of the manuscript, HK performed research and helped to write the manuscript, LGL performed research, PdV performed the electroretinograms, EJdR helped to write the manuscript, AMC and PB coordinated the research, supervised the project and wrote, edited and revised the manuscript.

Supplementary information listing Includes 4 supplementary figures

Introduction

Autophagy is a catabolic process by which cells degrade intracellular components inside lysosomes (Mizushima *et al.* 2008). Three main autophagic pathways have been described in mammalian cells, macroautophagy, microautophagy and chaperone-mediated autophagy (CMA). During macroautophagy parts of the cytosol including whole organelles are enclosed in a double membrane structure named autophagosome that then fuses with lysosomes to degrade the enclosed material (Mizushima *et al.* 2008). In CMA, specific cytosolic soluble proteins bearing a targeting motif are recognized by a chaperone that delivers them to the lysosomal receptor the lysosome-associated membrane protein type 2A (LAMP-2A) for translocation into the lysosomal lumen (Cuervo 2010). Macroautophagy and CMA are maximally activated under stress conditions but basal activity for these pathways is also detected in most cell types. Previous studies in cultured cells have suggested the existence of a bidirectional crosstalk between these two pathways as macroautophagy is upregulated after CMA blockage (Massey *et al.* 2008) and CMA is induced in cells with macroautophagy compromise (Kaushik *et al.* 2008). While the role of autophagy in the maintenance of cell and tissue homeostasis is well documented (Mizushima *et al.* 2008), the relative contributions of the different autophagic pathways in retinal pathophysiology remains unknown (Boya In press).

Genetic inhibition of autophagy induces degenerative changes in mammalian tissues that resemble those associated with aging, and normal and pathological aging are often associated with a reduced autophagic potential (Cuervo 2008). The role of autophagy in the nervous system is a matter of intense investigation as these pathways are often missregulated during neurodegenerative conditions and autophagy manipulation could represent a new approach to cure these devastating diseases (Harris & Rubinsztein 2012). Little is know about the role of autophagy in the retina. We have recently shown that autophagy protects retinal ganglion cells after axonal damage in vivo (Rodriguez-Muela *et al.* 2012) and that it helps to maintain ATP levels during retinal development (Boya *et al.* 2008; Mellén *et al.* 2008).

Retinal aging is often associated to a decrease in visual acuity, ocular accommodation and dark adaptation. In addition, this aging phenotype is aggravated by several diseases such as age-dependent macular degeneration (AMD), cataracts, glaucoma and diabetic retinopathy, causing blindness. AMD, the leading cause of vision loss in the elderly world-wide (Lim *et al.* 2012), is characterized by morphological and functional abnormalities in the retinal pigmented epithelium (RPE), that often lead to their cell death causing the secondary adverse effects in the neural retina and ultimately, the loss of vision (Kaarniranta *et al.* 2009). Recent evidence demonstrating an increased autophagy activity in the aging RPE and the presence of autophagy markers in the extracellular protein deposits in the eyes of human donors with AMD (Wang *et al.* 2009a) has led to the hypothesis that autophagy plays a pathogenic role in AMD (Wang *et al.* 2009b). Conversely, impaired autophagy in RPE cells also results in increased lipofuscinogenesis in vitro (Krohne *et al.* 2010). However, the impact of autophagy in age-related retinal dysfunction is still unknown.

The most abundant cell types in the retina are photoreceptor cells, rods and cones, which are in charge of sensing light and start the phototransduction cascade. Rods are used for low-light vision and cones for daylight, bright-colored vision. Damage to photoreceptors contributes to the gradual loss of sight associated with physiological aging and retinopathies resulting in blindness. Age-related alterations in the ubiquitin-proteasome system have been extensively described in the central nervous system, including the retina (Shang & Taylor

2012). However, concomitant changes in the lysosomal-autophagic system, the other major system for cellular quality control, are less well characterized.

In this work, we have identified a marked reduction in macroautophagy activity with age in the retina, which coincides with an increase in levels of several limiting components for chaperone-mediated autophagy (CMA). Inhibition of macroautophagy in retinal cells *in vivo* and *in vitro* induces robust upregulation of CMA in the compromised cells. However, in contrast to other cell types, the autophagic cross-talk in retinal cells is not bi-directional. We propose that cell type-dependent differences in the interplay in between autophagic pathways in the retina may be responsible for the specific pattern of visual lost in aging.

Results

Macroautophagy is the best characterized autophagic pathway in mammals (Mizushima *et al.* 2008). Using mouse retinas, a highly accessible part of the central nervous system, we compared levels of macroautophagy at different ages. No significant differences in the basal steady-state levels of LC3-II, an integral component of the autophagosome membrane (Tanida *et al.* 2005), were observed in aged animals (Fig. 1A). However, when studying the autophagy flux -determined as the change in the levels of LC3-II in the presence and in the absence of lysosomal inhibitors- we observed that in the older animals (12 and 22 months old) LC3-II levels did not significantly increase after the lysosomal blockage compared to the young ones (Figure 1A, B). The inferred age-related decrease in autophagosome formation was supported by a reduction in mRNA levels of *Beclin1*, a regulatory component of the autophagy initiation complex, and *Atg7,* the rate-limiting enzyme mediating elongation of the autophagosome membrane (Fig. 1C). This decrease in the mRNA expression is correlated with changes in Beclin1 protein levels by immunoflourescence in animals of 22 months of age in comparison with young animals (Fig. 1D). Moreover, we observed a concomitant transcription-independent increase in protein levels of p62, a well-described macroautophagy substrate (Fig. 1E-G). Ultrastructural analysis of the aged retinas revealed no significant expansion of autophagy-related compartments (Supp. Fig. 1A), further supporting the data that the main defect in macroautophagy occurs at the level of autophagosome formation and not during the degradation phase. Aged retinas exhibited lipofuscin-loaded lysosomes and electron-dense aggregates, compatible with inefficient removal of cytosolic cargo by macroautophagy and severe alterations in cellular quality control (Fig 2A and Supp. Fig. 1B, Fig 2A). Some of the inclusions were of proteinaceous nature, as revealed by ubiquitin immunostaining, which was detected throughout all layers of aged retinas (Fig 2B). The observed reduction in macroautophagy in the retinas of the old animals was accompanied by several degenerative features, including reduced number of photoreceptor cells in the ONL (Supp. Fig. 1C), altered structure of the outer segments of photoreceptors (Supp. Fig. 1D), and increased numbers of apoptotic cells (Supp. Fig. 1E). Although a significant compromise of macroautophagy (reduced LC3 flux and p62 accumulation) was only evident in the 22 months old group, we found a gradual trend toward declined activity in the middle age group. The fact that the ultra structural analysis did not reveal marked changes between 3 and 12 months old mice (Fig. Sup 1 C, E) supports that cells may activate responses to compensate for this gradual loss in autophagic function and to preserve cellular homeostasis.

Generalized lysosomal failure has been associated with age-related neurodegeneration (Dehay *et al.* 2010; Wong & Cuervo 2010). Unexpectedly, we detected a dramatic increase in total proteolysis of long-lived proteins in retinal explants from aged animals (Fig. 3A). This increase in degradative capacity was independent of the proteasome, as even in the presence of proteasome inhibitors, higher proteolysis rates were still evident in aged retinas as compared with younger ones (Supp. Fig. 2A). These observations suggest the

upregulation of a lysosomal pathway other than macroautophagy in aged retinas. Upregulation of chaperone-mediated autophagy (CMA), the other stress-induced autophagic pathway in mammals (Cuervo 2010), has been previously described *in vitro* in macroautophagy-deficient cell lines (Kaushik *et al.* 2008). We thus analyzed the levels of LAMP-2A, a limiting component required for CMA. Levels of both LAMP-2A and Hsc70, the chaperone that participates lysosomal delivery of CMA substrates, were increased in aged versus young retinas (Fig 3B, and Supp. Fig. 2B,C). This finding supports that the observed increase in lysosomal-dependent proteolysis may indeed be a result of the upregulation of CMA in aged retinas.

The age-related increase in retinal CMA markers noticeable contrasts with the decreased activity of this pathway that occurs in other organs with age (Cuervo & Dice 2000; Zhang & Cuervo 2008), and may indicate a prominent role for CMA in the retina when macroautophagy is compromised. To address this possibility, we downregulated the expression of Atg7 or LAMP-2A, essential proteins for macroautophagy and CMA respectively, by shRNA-mediated knock-down (KD) in 661W photoreceptor cells. CMA blockade resulted in a marked reduction in basal proteolysis rates in 661W cells, while compromised macroautophagy (Atg7 KD) resulted in increased proteolysis as compared with control cells, in agreement with our *in vivo* findings (Fig. 3C). This increase in proteolysis is likely due to the upregulated CMA activity, measured by means of a photo-switchable fluorescent reporter KFERQ-PA-mCherry1 (Koga *et al.* 2011), that we found in Atg7 KD cells. Blockage of macroautophagy in 661W cells results in a significant increase on basal CMA activity but not further activation when this pathway is upregulated by removal of nutrients in the culture media (Fig. 3D). As expected, LAMP-2A KD cells displayed reduced CMA activity, confirming the validity of this reporter assay (Fig. 3D; prolonged serum removal, a well-characterized stimulus of CMA, was used as a positive control). As expected Atg7 knockdown reduced autophagic flux by westernblot and by counting LC3 dots after immunofluorescence (Fig 3E, F).

Analysis of possible changes in macroautophagy in response to the CMA blockage in these cells revealed that, contrary to the upregulation of macroautophagy observed in most cell types in response to CMA blockage (Massey *et al.* 2008), CMA down-regulation in 661W cells did not increase macroautophagy activity (Fig. 3E, F). This inability to upregulate macroautophagy upon CMA blockage may explain the higher sensitivity to oxidative stress observed in the 661W L2AKD cells as increased cell death after paraquat treatment (Fig. 3G). Moreover, this high dependence on proper functioning of autophagic pathways for maintenance of homeostasis appeared to be specific to photoreceptor-derived cells. Thus downregulation of Atg7 or LAMP-2A in RGC-5 immortalized retinal ganglion cells had no significant effect on proteolysis (Fig. 3C), supporting a possible higher contribution of the activity of the ubiquitin/proteasome system to intracellular degradation in these cells. Interestingly, despite this lower participation of autophagic pathways to proteolysis, and as a difference with 661W cells, RGC-5 cells showed the expected bi-directional crosstalk between macroautophagy and CMA. RGC-5 cells increased autophagic flux after L2A knockdown (Sup Fig 3A) and respond to blockage of macroautophagy by upregulating CMA under basal conditions (Suppl. Fig. 3B).

Overall, these results support the existence of cell type-dependent differences on the contribution of autophagic and non-autophagic pathways to retinal homeostasis and in the cross-talk among these pathways. Thus, we have demonstrate that whereas ablation of macroautophagy in cone photoreceptor cells results in the expected increased CMA activity, CMA downregulation does not lead to increased macroautophagy, demonstrating that the crosstalk between autophagic pathways in this cell type is unidirectional.

To further assess the impact of macroautophagy downregulation in the retina *in vivo* and to determine whether the observed age-related changes in CMA were secondary to altered macroautophagic function, we studied conditional *Atg5* knockout mice generated by crossing of $Atg5^{flox/flox}$ with nestin-*Cre* mice. These mice display ubiquitin-positive inclusions in several neuronal types, as well as motor deficits and neurodegeneration (Hara *et al.* 2006), though their retinal phenotype has not been characterized to date. Like aged animals, conditional *Atg5* knockout mice displayed increased levels of p62 and ubiquitinated proteins in the retina (Fig. 4A). Moreover, levels of both LAMP-2A and Hsc70, were also increased in the retina of *Atg5*-deficient mice (Fig. 4 A-C), supportive of compensatory activation of CMA.

Next, we analyzed the consequences of macroautophagy blockade in retinal homeostasis. TUNEL-positive apoptotic nuclei were observed in the photoreceptor layer of conditional *Atg5* knockout mice (Fig. 4D, E), as well as elevated levels of phosphorylated Tau (Fig. 4F), reproducing the increase observed in the aged retinas (Sup Fig. 4). Together with the histological signs of neurodegeneration, *Atg5* deficient mice also presented a clear decline in their visual function (Fig. 5A). Electroretinograms (ERG) selectively associated with scotopic tests (STR, b-scot, a-mixed and OP), indicative of rod function, revealed a reduction in scotopic/dim-light vision in these mice by 7 weeks of age, comparable with that described in aged mice (Kolesnikov *et al.* 2010). We postulate that cone function is preserved in these animals due to the increased contribution of CMA in these cells. In support of this view, TUNEL-positive cells in the retinas of conditional *Atg5* knockout mice were negative for three different cone markers (Fig. 5B, C).

In summary, our studies have identified the existence of cross-talk between the two principal types of autophagy, macroautophagy and CMA in the retina *in vivo*. Communication between these two autophagic systems helps eliciting compensatory mechanisms, which contribute to maintain cellular homeostasis when one of the pathways is compromised.

Discussion

In this work, we describe a primary dysfunction of macroautophagy in the retina of aged mice, which contributes to the age-associated reduction of visual function and to retinal dystrophy. We have also confirmed, for the first time *in vivo,* the existence of cross-talk between different autophagic pathways and provide an example of the physiological relevance of the intercommunication between macroautophagy and CMA. Thus, the robust compensatory activation of CMA observed in cone retinal cells when macroautophagy is experimentally blocked is likely behind the higher resistance of these cells to the functional loss of macroautophagy observed with age (Kolesnikov *et al.* 2010).

A combination of defects in autophagosome formation and clearance contributes to the reduced macroautophagy activity with age described in organs such as liver, kidney, heart and some brain regions (Cuervo & Dice 2000). Ultrastructural analysis of the aged retinas revealed no significant expansion of autophagy-related compartments suggesting that, in clear contrast with these other organs, the main defect in macroautophagy occurs at the level of autophagosome formation and not during the degradation phase. Interestingly, although the defect in macroautophagy function is already detectable at 12 months of age, the degenerative phenotypes in the retina are not fully evident until later ages, supporting the importance of the activation of compensatory mechanisms, such as the CMA upregulation described in this work, that help preserving retinal homeostasis even when macroautophagy is defective. Future studies are necessary to determine the cause of the transcriptional downregulation of essential autophagy components such as Beclin-1 and Atg7 observed in

the aged retina and whether they are solely responsible for the reduction in autophagosome biogenesis in this tissue.

It is noteworthy that contrary to other cell types, the cross-talk between autophagic pathways in photoreceptor cells is unidirectional. Whereas macroautophagy downregulation leads to a robust enhancement of CMA activity, in agreement with our observations in aged retina, macroautophagy is not activated in these cells in response to CMA blockade, leaving these cells vulnerable to stressors such as oxidative stress. We have only found a similar inability to upregulate macroautophagy in response to CMA inhibition in the case of cancer cells, which coincidently show high basal levels of CMA activity, similar to the ones that we describe here for retinal cells (Kon *et al.* 2011). Disruption of the autophagic cross-talk may be necessary to support the observed constitutive activation of CMA in retinal cells.

The increase in CMA activity observed in the aging retina is unprecedented, as in most organs the activity of this autophagic pathway declines with age (Cuervo & Dice 2000; Zhang & Cuervo 2008). Upregulation of CMA in the retina of old animals, could be reactive to a loss of macroautophagic activity with age, and may exert a protective effect, as the one that we observed in the cone cells of conditional Atg5 knockout mice. Alternatively, CMA activation in the old retina may reflect a generalized response of retinal cells to stress; indeed, transcriptional upregulation of LAMP-2A was recently described in a model of retinitis pigmentosa (Punzo *et al.* 2009). Both, the inability of some retinal cells to upregulate CMA in response to macroautophagic blockage, and the higher dependence of some cell types on macroautophagy, could make CMA upregulation insufficient to compensate for the gradual loss of macroautophagy with age, eventually leading to their functional failure.

We have found that 661W cells, a cone-derived cell line, are very dependent on CMA for survival after oxidative stress (Fig. 3G). *In vivo*, cone markers never colocalize with TUNEL staining after genetic ablation of macroautophagy. It is thus tempting to speculate that a compensatory increase in CMA would make cones more resistant to stress in comparison with other retinal cell types, such as rods. Indeed, rods are the first to degenerate in most retinal dystrophies (Organisciak & Vaughan 2010) and after light induced damage in albino mice (Kunchithapautham *et al.* 2011). Moreover, being responsible for night vision and dark adaptation, photoreceptor rod loss is one of the first consequences of physiological aging (Kolesnikov *et al.* 2010). We find a reduction in rod-associated electroretinograms after macroautophagy ablation in agreement with the increased vulnerability of those cells in many pathological settings, including aging. Thus the differential capability of retinal cells to upregulate CMA or macroautophagy may be behind the observed decrease in retinal function during physiological and pathological conditions.

In this work we have characterized for the first time the retinal phenotype of an autophagy-deficient animal model. Our data show the presence of protein aggregates as has been observed in other parts of the central nervous system in those animals at similar ages such as the cerebral cortex, the hippocampus and the thalamus (Hara *et al.* 2006). In addition, TUNEL-positive cells are found in the nuclear layer of photoreceptors at P52. Other cell types shown to be affected by apoptotic cell death in these autophagy-deficient mice are the granular cells of the cerebellum at 6 weeks of age (Hara *et al.* 2006). Interestingly, although the gross morphology of the retina is maintained, we find severe deficits in night vision indicating that proper autophagy is essential to keep retinal function in the absence of major structural abnormalities. This is in contrast to other types of retinal degeneration where a marked reduction in the number of photoreceptor cells does not have a great impact in electroretinographic responses (Corrochano *et al.* 2008).

In conclusion, our study reveals the occurrence of tissue-dependent, and even of cell type-dependent differences in the autophagic pathway primarily affected with aging and in the capability to compensate for this defect by upregulating a different autophagic pathway. In the case of the retina, these differences provide a plausible explanation for the specific pattern of sight loss with age.

Experimental procedures

All animal procedures were approved by the local ethics committee for animal experimentation, under animal study protocols approved by the Albert Einstein College of Medicine Animal Institute Animal Care and Use Committee and by the CSIC and were carried out in accordance with the American and European Union guidelines. C57BL/6J mice were obtained from The Jackson Laboratory (Bar Harbor, ME). *Atg5*$^{flox/flox}$ mice (Hara *et al.* 2006) were kindly provided by Noboru Mizushima (Tokyo Medical and Dental University, Japan). Nestin-*Cre* mice where provided by Marcos Malumbres at CNIO, Spain. Control animals are considered *Atg5*$^{+/flox}$; *nestin*-Cre the *Atg5*$^{flox/flox}$ and the *Atg5*$^{+/flox}$ as described in (Hara *et al.* 2006). Animals of either sex were used for this study. For the aging studies, 3- 12 and 22-month-old mice from the National Institute on Aging age-controlled colony were employed. Mice were maintained on a 12-h light/dark cycle in a temperature-controlled barrier facility, with free access to water and food.

ERG Recordings

Mice were dark adapted over night, and subsequent manipulations were performed in dim red light. Mice were anesthetized with intraperitoneal injections of ketamine (95 mg/kg) and xylazine (5 mg/kg) solution and maintained on a heating pad at 37°C. Pupils were dilated with a drop of 1% tropicamide (Colircusıi Tropicamida; Alcon Cusi, Barcelona, Spain). To optimize electrical recording, a topical drop (2% Methocel; Hetlingen, Switzerland) was instilled on each eye immediately before situating the corneal electrode. Flash induced ERG responses were recorded from the right eye in response to light stimuli produced with a Ganzfeld stimulator. Light intensity was measured with a photometer at the level of the eye (Mavo Monitor USB; Nürenberg, Germany). Four to 64 consecutive stimuli were averaged with an interval between light flashes in scotopic conditions of 10 seconds for dim flashes and of up to 60 seconds for the highest intensity. Under photopic conditions, the interval between light flashes was fixed at 1 second. ERG signals were amplified and band filtered between 0.3 and 1000 Hz with an amplifier (CP511 AC amplifier; Grass Instruments, Quincy, MA). Electrical signals were digitized at 20 kHz with a power laboratory data acquisition board (AD Instruments, Chalgrove, UK). Bipolar recording was performed between an electrode fixed on a corneal lens (Burian-Allen electrode; Hansen Ophthalmic Development Laboratory, Coralville, IA) and a reference electrode located in the mouth, with a ground electrode located in the tail. Under dark adaptation, scotopic threshold responses (STR) were recorded to light flashes of −4 log cd·s·m^{-2}; rod responses were recorded to light flashes of -2 cd·s·m^{-2}s and mixed responses were recorded in response to light flashes of 1.5 log cd·s·m^{-2}. Oscillatory potential (OP) was isolated using white flashes of 1,5 log cd·s·m^{-2} in a recording frequency range of 100 to 10,000 Hz. Under light adaptation, cone-mediated responses to light flashes of 2 log cd·s·m^{-2} on a rod-saturating background of 30 cd·m^{-2} were recorded. Wave amplitudes of the STR, rod responses (b-rod), mixed responses (a-mixed and b-mixed) and OP were measured off line by an observer masked to the experimental condition of the animal.

Cryosections, Inmunofluorescence and detection of apoptosis

Animals were euthanized by an overdose of sodium pentobarbital. Cryosections and immnufluorescence in retinal sections were perfomed as previsously described (Rodriguez-

Muela *et al.* 2012). Immunofluoresecence in 661W cells was performed as previously described (Vazquez *et al.* 2012). Primary antibodies used in this study were LC3 (MBL, MA, USA), p62 (Enzo, NY, USA), LAMP-2A (Invitrogen, CA, USA), Hsc70 (Stressgen, NY, USA), Ubiquitinated proteins (Santa Cruz), Opsin red/green (Chemicon), Opsin blue (Chemicon), Cone transducin (Cytosignal) and P-Tau (Thermoscientific, IL, USA). Sections were visualized by confocal microscopy (TCS SP2; Leica Microsystems, Wetzlar, Germany). Apoptosis was detected by TUNEL as described (Mellén *et al.* 2008) using the Apoptosis Detection System; Promega, Madison, WI, USA.

Transmission electron microscopy

TEM in whole retinas was performed as previously described (Rodriguez-Muela *et al.* 2012). Sectioning for electron microscopic examination followed was accomplished with an ultramicrotome (Vitracut E, Reichert-Jung, Austria) and electron microscopy was performed with a Zeiss EM 902 transmission electron microscope (Germany), at 90 kV, on ultra-thin sections (50 nm) stained with uranyl acetate and lead citrate. The quantification of the number of photoreceptor nuclei present in the ONL was performed on four different sections from at least three animals per group (3 versus 22 months old).

Semiquantitative and quantitative RT-PCR

RNA was isolated from individual retinas using Trizol (Invitrogen). Reverse transcription was performed on 1 μg of total RNA using Oligo (dT) and the Superscript III enzyme (Invitrogen) following the manufacturer's instructions. For q-PCR, 100 ng of the obtained cDNA were used and the assays were performed using the TaqMan Universal PCR Master mix (Roche Applied Biosystems, Basel, Switzerland), and probes were obtained from the Universal ProbeLibrary Set (Roche Applied Science). Amplifications were run in a 7900 HT-Fast Real-Time PCR System (Roche Applied Biosystems). Each value was adjusted by using GAPDH RNA levels as a reference. The primer sequences used were: beclin-1F 5′-caggcgaaaccaggagag-3′; beclin-1R 5′-cgagtttcaataaatggctcct-3′; lamp2aF 5′-gtgacaaaaggacagtattctacagc-3′, lamp2aR 5′-ccaataaaataagccagcaaca-3′; atg7F 5′-ccggtggcttcctactgtta-3′, atg7R 5′-aaggcagcgttgatgacc-3′; p62F 5′-gctgccctatacccacatct-3′, p62R 5′- cgccttcatccgagaaac-3′; 18SF 5′-tgcgagtactcaacaccaaca-3′, 18sR 5′-ttcctcaacaccacatgagc-3

Western blot

Western blot in retinas were performed as previously described (Mellén *et al.* 2009). Briefly, after removal of the eyes, neuroretinas were dissected free of other tissues and lysed in a buffer containing 50 mM Tris-HCl pH 6.8, glycerol 10% (v/v), 2% SDS (w/v), 10 mM DTT, and 0.005% bromophenol blue. Thirty micrograms of protein was resolved on a 15% SDS-PAGE gel and transferred to PVDF membranes (Bio-Rad, Hercules, CA, USA). The antibodies used were LC3 (MBL), p62 (Enzo), ubiquitinated proteins (Santa Cruz Biotechnology), LAMP-2A (Invitrogen), Hsc70 (Stressgen), β-actin (Sigma) and GAPDH (Abcam, Cambridge, UK). Antibodies were detected with the appropriate horseradish peroxidase-labelled secondary antibodies (Pierce, Rockford, IL, USA) and were visualized with the SuperSignal West Pico chemiluminescent substrate (Pierce). Densitometric analysis was performed with Quantity One software (Bio-Rad).

Cell culture

661W murine photoreceptor-derived cell line (Tan et al. 2004) was provided by Dr Muayyad Al-Ubaidi (Department of Cell Biology, University of Oklahoma Health Sciences Center, OK, USA). Mouse retinal ganglion cell line (RGC-5) (Krishnamoorthy et al. 2001; Van Bergen et al. 2009) and 661W cells were cultured in Dulbecco's Modified Eagle's

Medium (DMEM) 10% FBS, 1% penicillin/streptomycin in a 5% CO_2 incubator. LAMP-2A and Atg7-knockdown cells were generated by using a vector expressing GFP and shRNA and control cells are transfected with a non-silencing lentiviral vector expressing the unrelated protein PGK coupled to GFP to correct for the effects of lentiviral infection as previously described (Singh *et al.* 2009). For western blot analysis, 2×10^4 cells were plated in 6 well plates and exposed to the treatments for 24 h. Serum removal was performed by thoroughly washing the cells with Hanks' Balanced Salt Solution (Invitrogen) and placing them in serum-free complete medium. Cells were treated with the combination of 100 μM leupeptin (Thermo Fisher Scientific, MA, USA) plus 20 mM ammonium chloride (Sigma) for 4h to inhibit lysosomal proteolysis.

Intracellular Protein Turnover

Rates of protein synthesis were measured in retinal explants or in confluent cells as the incorporation of [^{3}H]leucine [10 mCi/ml (1 Ci = 37 GBq)] into acid-insoluble material in the presence of an excess (2.8 mM) of unlabeled leucine in the medium (to minimize differences due to alteration of amino acid transport and/or intracellular amino acid pool sizes). To measure degradation of long-lived proteins, retinas or confluent cells were labelled with [3H]leucine (2 mCi/ml) for 48 h at 37°C and extensively washed. Retinas were maintained in R16 medium (provided by Dr P. A. Ekstrom, Wallenberg Retina Centre, Lund University, Lund, Sweden) and cell lines in DMEM containing an excess of unlabelled leucine, and treated with 5 μM lactacystin (Calbiochem, Darmstadt, Germany) or 20 mM ammonium chloride (Sigma) plus 100 μM leupeptin when indicated. Aliquots of the medium at different times were precipitated with trichloroacetic acid, and proteolysis was expressed as the percentage of the initial acid-insoluble radioactivity (protein) transformed into acid-soluble radioactivity (amino acids and small peptides) at the end of the incubation. Total radioactivity incorporated into cellular proteins was determined as the amount of acid-precipitable radioactivity in labeled cells immediately after washing.

CMA activity assays, construction of the reporter plasmids, photoconversion and imaging procedures

The pKFEFQ-PA-mCherry plasmid construction and the establishment of stable cell lines expressing the CMA reporter was performed by using lentiviral transfer vectors as described (Koga *et al.* 2011). Photoconversion of cells grown on coverslips was carried out with a 405/20 nm LED array (Norlux) for 10 min using 50 mW cm^{-2} light intensity. More than 90% of the cells were viable after the photoconversion. All images were acquired with an Axiovert 200 inverted fluorescence microscope (Zeiss, Oberkochen, Germany). A sufficient number of fields were acquired to analyze at least 40 cells per well. Images were analyzed with Image J software (NIH).

Quantification of LC3 puncta by image analysis

LC3 puncta were quantified after immunofluorescence for LC3 (Nanotools, Teningen, Germany) using the web-based image analysis tool WimAutophagy of Wimasis (www.wimasis.com) on at least 300 cells per treatment. This online software tool is able to recognize fluorescent puncta and associate them to each nucleus as well as to recognize GFP-positive (knockdown cells) and GFP-negative cells (non-transfected cells). Graphs display the number of puncta per cell in GFP-positive cells.

Statistical analysis

Results are expressed as mean ± SE. Statistical analysis was performed using the JMP IN 4.0.3 software. For most analyses we used one-way ANOVAs with treatment as a fixed factor. For analysis in figure 1B and 3E, D and Supp. Fig 3C 2-way ANOVAs where

performed with the factors treatment and age or cell type respectively. All interactions were non-significant. For significantly different factors, comparisons among factor levels were performed using posthoc Tuckey tests. If assumptions of normality and homoscedasticity were not met, we applied non-parametric tests. For all tests the significance level was $p<0.05$ (2-tailed) and multiple testing was accounted for using Bonferroni correction

Supplementary Material

Refer to Web version on PubMed Central for supplementary material.

Acknowledgments

This work was supported by grants from MINECO (Spain), SAF-2009-08086 to PB, and CONSOLIDER CSD2010-000454 to PB and EJdR, and from NIH (AG031782 and AG038072) to AMC. NRM was a recipient of a FPU fellowship from MICINN. We thank Dr. Teresa Suárez for her helpful comments and discussion. The authors declare no conflict of interests.

References

Boya, P.; Yue, Z.; Chu, CT. Neuronal Autophagy: A life-and- death affair. World Scientific Publishing Co; (In press)

Boya P, Mellen MA, de la Rosa EJ. How autophagy is related to programmed cell death during the development of the nervous system. Biochem Soc Trans. 2008; 36:813–817. [PubMed: 18793142]

Corrochano S, Barhoum R, Boya P, Arroba AI, Rodriguez-Muela N, Gomez-Vicente V, Bosch F, de Pablo F, de la Villa P, de la Rosa EJ. Attenuation of vision loss and delay in apoptosis of photoreceptors induced by proinsulin in a mouse model of retinitis pigmentosa. Invest Ophthalmol Vis Sci. 2008; 49:4188–4194. [PubMed: 18515565]

Cuervo AM. Autophagy and aging: keeping that old broom working. Trends Genet. 2008; 24:604–612. [PubMed: 18992957]

Cuervo AM. Chaperone-mediated autophagy: selectivity pays off. Trends Endocrinol Metab. 2010; 21:142–150. [PubMed: 19857975]

Cuervo AM, Dice JF. Age-related decline in chaperone-mediated autophagy. J Biol Chem. 2000; 275:31505–31513. [PubMed: 10806201]

Dehay B, Bove J, Rodriguez-Muela N, Perier C, Recasens A, Boya P, Vila M. Pathogenic lysosomal depletion in Parkinson's disease. J Neurosci. 2010; 30:12535–12544. [PubMed: 20844148]

Hara T, Nakamura K, Matsui M, Yamamoto A, Nakahara Y, Suzuki-Migishima R, Yokoyama M, Mishima K, Saito I, Okano H, Mizushima N. Suppression of basal autophagy in neural cells causes neurodegenerative disease in mice. Nature. 2006; 441:885–889. [PubMed: 16625204]

Harris H, Rubinsztein DC. Control of autophagy as a therapy for neurodegenerative disease. Nat Rev Neurol. 2012; 8:108–117. [PubMed: 22187000]

Kaarniranta K, Salminen A, Eskelinen EL, Kopitz J. Heat shock proteins as gatekeepers of proteolytic pathways-Implications for age-related macular degeneration (AMD). Ageing Res Rev. 2009; 8:128–139. [PubMed: 19274853]

Kaushik S, Massey AC, Mizushima N, Cuervo AM. Constitutive activation of chaperone-mediated autophagy in cells with impaired macroautophagy. Mol Biol Cell. 2008; 19:2179–2192. [PubMed: 18337468]

Koga H, Martinez-Vicente M, Macian F, Verkhusha VV, Cuervo AM. A photoconvertible fluorescent reporter to track chaperone-mediated autophagy. Nat Commun. 2011; 2:386. [PubMed: 21750540]

Kolesnikov AV, Fan J, Crouch RK, Kefalov VJ. Age-Related Deterioration of Rod Vision in Mice. The Journal of neuroscience. 2010; 30:11222–11231. [PubMed: 20720130]

Kon M, Kiffin R, Koga H, Chapochnick J, Macian F, Varticovski L, Cuervo AM. Chaperone-mediated autophagy is required for tumor growth. Sci Transl Med. 2011; 3:109ra117.

Krishnamoorthy RR, Agarwal P, Prasanna G, Vopat K, Lambert W, Sheedlo HJ, Pang IH, Shade D, Wordinger RJ, Yorio T, Clark AF, Agarwal N. Characterization of a transformed rat retinal ganglion cell line. Brain Res Mol Brain Res. 2001; 86:1–12. [PubMed: 11165366]

Krohne TU, Stratmann NK, Kopitz J, Holz FG. Effects of lipid peroxidation products on lipofuscinogenesis and autophagy in human retinal pigment epithelial cells. Exp Eye Res. 2010; 90:465–471. [PubMed: 20059996]

Kunchithapautham K, Coughlin B, Lemasters JJ, Rohrer B. Differential Effects of Rapamycin on Rods and Cones During Light-Induced Stress in Albino Mice. Investigative ophthalmology & visual science. 2011; 52:2967–2975. [PubMed: 21273550]

Lim LS, Mitchell P, Seddon JM, Holz FG, Wong TY. Age-related macular degeneration. Lancet. 2012; 379:1728–1738. [PubMed: 22559899]

Massey AC, Follenzi A, Kiffin R, Zhang C, Cuervo AM. Early cellular changes after blockage of chaperone-mediated autophagy. Autophagy. 2008; 4:442–456. [PubMed: 18253088]

Mellén MA, de la Rosa EJ, Boya P. The autophagic machinery is necessary for removal of cell corpses from the developing retinal neuroepithelium. Cell Death Differ. 2008; 15:1279–1290. [PubMed: 18369370]

Mellén MA, de la Rosa EJ, Boya P. Autophagy is not universally required for phosphatidyl-serine exposure and apoptotic cell engulfment during neural development. Autophagy. 2009; 5:964–972. [PubMed: 19587526]

Mizushima N, Levine B, Cuervo AM, Klionsky DJ. Autophagy fights disease through cellular self-digestion. Nature. 2008; 451:1069–1075. [PubMed: 18305538]

Organisciak DT, Vaughan DK. Retinal light damage: Mechanisms and protection. Progress in Retinal and Eye Research. 2010; 29:113–134. [PubMed: 19951742]

Punzo C, Kornacker K, Cepko CL. Stimulation of the insulin/mTOR pathway delays cone death in a mouse model of retinitis pigmentosa. Nat Neurosci. 2009; 12:44–52. [PubMed: 19060896]

Rodriguez-Muela N, Germain F, Marino G, Fitze PS, Boya P. Autophagy promotes survival of retinal ganglion cells after optic nerve axotomy in mice. Cell Death Differ. 2012; 19:162–169. [PubMed: 21701497]

Shang F, Taylor A. Roles for the ubiquitin-proteasome pathway in protein quality control and signaling in the retina: implications in the pathogenesis of age-related macular degeneration. Mol Aspects Med. 2012; 33:446–466. [PubMed: 22521794]

Singh R, Kaushik S, Wang Y, Xiang Y, Novak I, Komatsu M, Tanaka K, Cuervo AM, Czaja MJ. Autophagy regulates lipid metabolism. Nature. 2009; 458:1131–1135. [PubMed: 19339967]

Tan E, Ding XQ, Saadi A, Agarwal N, Naash MI, Al-Ubaidi MR. Expression of cone-photoreceptor-specific antigens in a cell line derived from retinal tumors in transgenic mice. Invest Ophthalmol Vis Sci. 2004; 45:764–768. [PubMed: 14985288]

Tanida I, Minematsu-Ikeguchi N, Ueno T, Kominami E. Lysosomal turnover, but not a cellular level, of endogenous LC3 is a marker for autophagy. Autophagy. 2005; 1:84–91. [PubMed: 16874052]

Van Bergen NJ, Wood JP, Chidlow G, Trounce IA, Casson RJ, Ju WK, Weinreb RN, Crowston JG. Recharacterization of the RGC-5 retinal ganglion cell line. Invest Ophthalmol Vis Sci. 2009; 50:4267–4272. [PubMed: 19443730]

Vazquez P, Arroba AI, Cecconi F, de la Rosa EJ, Boya P, De Pablo F. Atg5 and Ambra1 differentially modulate neurogenesis in neural stem cells. Autophagy. 2012; 8:187–199. [PubMed: 22240590]

Wang AL, Lukas TJ, Yuan M, Du N, Tso MO, Neufeld AH. Autophagy and exosomes in the aged retinal pigment epithelium: possible relevance to drusen formation and age-related macular degeneration. PLoS One. 2009a; 4:e4160. [PubMed: 19129916]

Wang AL, Lukas TJ, Yuan M, Du N, Tso MO, Neufeld AH. Autophagy, exosomes and drusen formation in age-related macular degeneration. Autophagy. 2009b; 5:563–564. [PubMed: 19270489]

Wong E, Cuervo AM. Autophagy gone awry in neurodegenerative diseases. Nat Neurosci. 2010; 13:805–811. [PubMed: 20581817]

Zhang C, Cuervo AM. Restoration of chaperone-mediated autophagy in aging liver improves cellular maintenance and hepatic function. Nat Med. 2008; 14:959–965. [PubMed: 18690243]

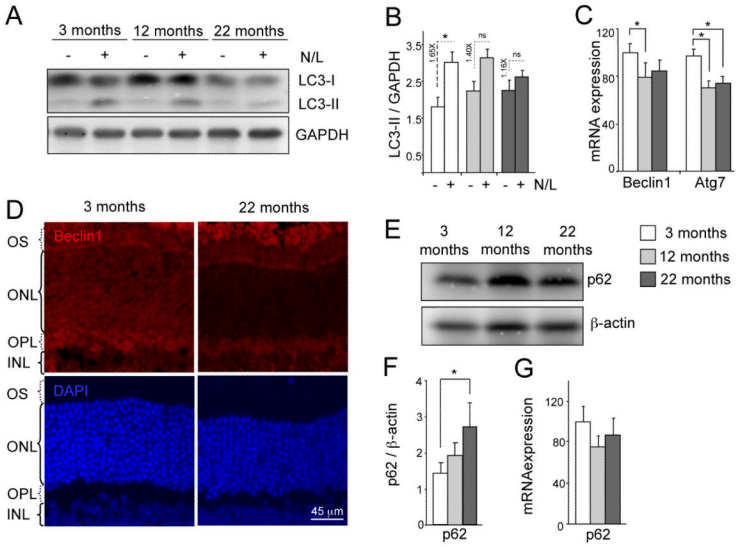

Figure 1.

Impaired macroautophagy in the aged mouse retina**.** (A) Autophagic flux as determined by western blot of LC3 in whole retinal extracts from mice of different ages in the absence/presence of the lysosomal inhibitors ammonium chloride and leupeptin (N/L). (B) Densitometric quantification of LC3-II in A and autophagic flux determined as the ratio of LC3-II in the presence/absence of lysosomal inhibitors (dotted lines) (n = 10). (C) *Beclin1* and *Atg7* mRNA expression as determined by qPCR. GAPDH is used as housekeeping gene (n = 6). (D) Beclin1 immnunostaining (red) in retinal sections from 3 and 22 months old animals. DAPI is used as nuclear stain (blue). (E, F) Western blot for p62, and its densitometric quantification, of retinal extracts from 3, 12 and 22 month-old mice showing increase of p62 levels with age (n = 10). (G) mRNA expression by qPCR of *p62* in retinal extracts from 3, 12 and 22 month-old animals (n = 6). *p<0.05.

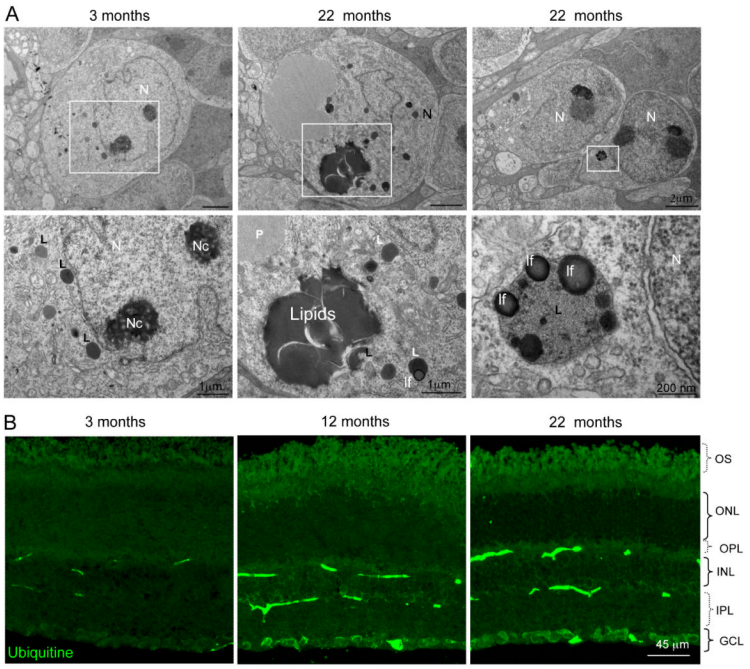

Figure 2.

Presence of lipofuscin and ubiquitin aggregates in aged retinas. (A) Accumulation of lipids, lipofuscin and proteinaceous material in the INL of 22 month-old retinas. Lower panels in A represent the area highlighted inside the white box. N, nucleus; Nc, nucleolus; lf, lipofuscin; L, lysosome; P, proteinaceous material. (B) Representative immunofluorescence for ubiquitin in retinal cryosections from 3, 12 and 22 month-old mice. GCL, ganglion cell layer; INL, inner nuclear layer; IPL, inner plexiform layer; ONL, outer nuclear layer; OPL, outer plexiform layer; OS, outer segment. Scale bars as depicted.

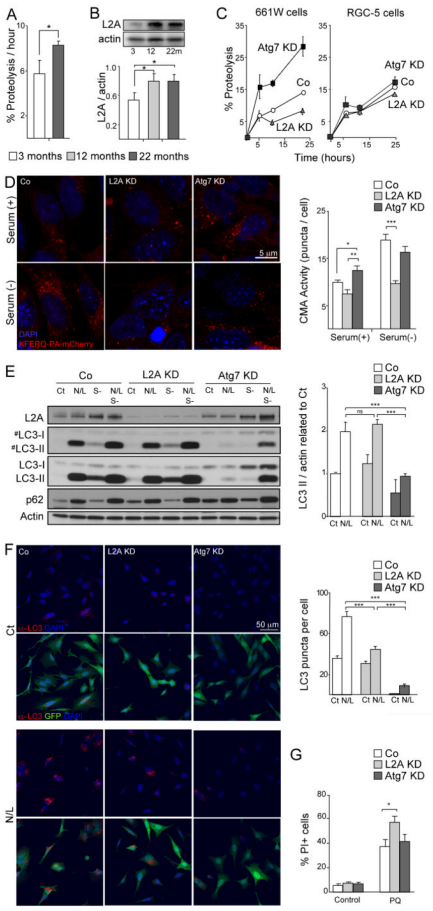

Figure 3.

Perturbation of macroautophagy results in increased CMA. (A) Retinal proteolytic rates of long-lived proteins determined by metabolic labeling of the indicated ages mice retinas (n = 5), *p<0.05. (B) Western blot for LAMP-2A in the same samples and densitometric quantification (n = 10); *p<0.05. (C) Proteolysis determined as in A in 661W and RGC-5 cells in control (Co) and after Atg7 or LAMP-2A knockdown (KD) at the indicated times of the chase period (n=4). (D) CMA activity as determined with the fluorescent reporter KFERQ-PA-mCherry in control, Atg7 and LAMP-2A KD 661W cells maintained in the presence of serum (+) or in the absence of serum (-) for 16h. Representative images (left) and quantification of the number of puncta per cell (right) are shown. Scale bar as depicted. *p<0.05, ** p<0.01, ***p<0.005. (E) Autophagic flux as determined by western blot of LC3 in the same cell lines maintained in the presence or absence of serum and of the lysosomal inhibitors ammonium chloride and leupeptin (N/L). Left: representative immunoblot (#) lower exposure time immunoblot. Right: Densitometric quantification of LC3-II in A and autophagic flux determined as the ratio of LC3-II in the presence/absence of lysosomal inhibitors (n = 3). ***p<0.005. (F) Immunofluorescence of LC3 in the same cells maintained in the presence or absence of N/L. Left: top panels show LC3 (red) and DAPI (blue) channels. Bottom panels include GFP channel (green) to track the knocked down cells. Right: Quantification of the number of LC3 positive puncta per cell (n>300 cells). ***p<0.005. (G) Cell viability as determined by propidium iodine (PI) staining and flow cytometry in control, Atg7 and LAMP-2A KD 661W treated with or without 150 μM paraquat (PQ) (n = 10). *p<0.05.

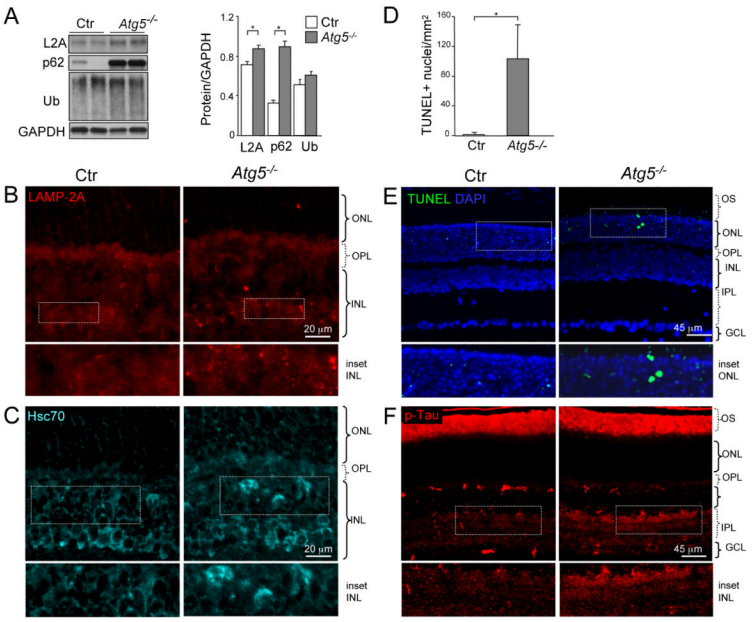

Figure 4.

Increased expression of CMA markers and signs of retinal damage in *Atg5*$^{flox/flox}$; nestin-*Cre* mice at 7 weeks of age. (A) Western blot for LAMP-2A, p62 and ubiquitin of total retinal extracts from control (Ctr) and *Atg5*$^{flox/flox}$; nestin-*Cre* (Atg5$^{-/-}$) mice (n = 6). (B-C) Staining for LAMP-2A and Hsc70. (D-E) TUNEL staining and its quantification in retinal sections. (F) Staining for p-Tau in representative retinal cryosections from control and *Atg5*$^{flox/flox}$; nestin-*Cre* mice. White boxed areas are shown at higher magnification below of each panel. GCL, ganglion cell layer; INL, inner nuclear layer; IPL, inner plexiform layer; ONL, outer nuclear layer; OPL, outer plexiform layer; OS, outer segment. *p<0.05. Scale bars as depicted.

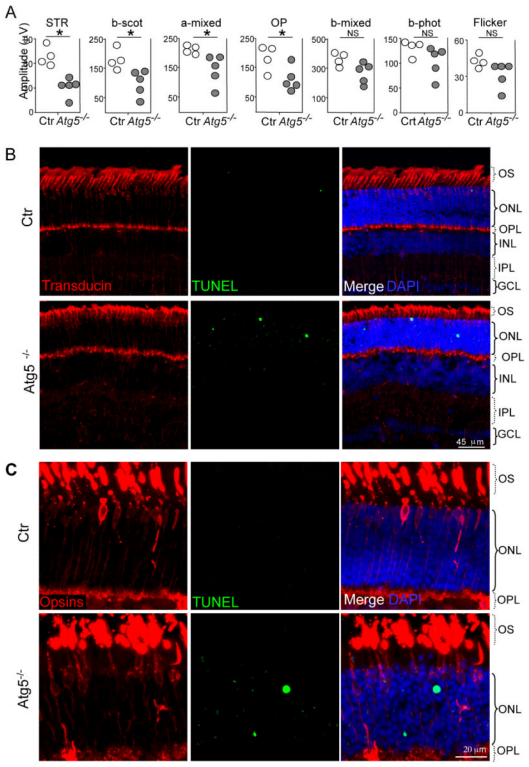

Figure 5.

Decreased rod function and apoptotic cell death in the photoreceptor layer of *Atg5*$^{flox/flox}$; nestin-*Cre* mice (A) Electroretinograms in control (Ctr) and *Atg5*$^{flox/flox}$; nestin-*Cre* mice (Atg5$^{-/-}$) (n = 5). STR, scotopic threshold potential; OP, oscilatory potentials. *p<0.05 *vs.* Ctr. (B-C) Representative immunostaining for cones in retinal cryosections from control (Ctr) and *Atg5*$^{flox/flox}$; nestin-*Cre* (Atg5$^{-/-}$) mice at 7 weeks of age by means of three different antibodies: (B) transducin (red) and (C) the combination of blue and red/green opsins (red). Apoptotic cells are stained by TUNEL (green). OS, outer segment; ONL, outer nuclear layer; OPL, outer plexiform layer; INL, inner nuclear layer; IPL, inner plexiform layer; and GCL, ganglion cell layer. Scale bars as depicted.